PSFC/JA-07-23

Full wave simulations of lower hybrid waves in toroidal geometry with Non-Maxwelian electrons

Wright, J.C., Valeo, E.J. [*], Phillips, C.K. [*], Bonoli, P.T., Brambilla, M. [**]

* Princeton Plasma Physics Laboratory
** Max Planck Institute for Plasma Physics, Garching, Germany

2007

**Plasma Science and Fusion Center
Massachusetts Institute of Technology
Cambridge MA 02139 USA**

Full wave simulations of lower hybrid waves in toroidal geometry with non-Maxwellian electrons

J. C. Wright[1][*], E. J. Valeo[2], C. K. Phillips[2], P. T. Bonoli[1], and M. Brambilla[3]

[1] *MIT - Plasma Science Fusion Center, Cambridge, MA, USA*

[2] *Plasma Physics Laboratory, Princeton, NJ, USA*

[3] *Max Planck Institute for Plasma Physics Garching, Germany*

---

[*]Corresponding author. *Email addresses:* `jwright@psfc.mit.edu` (J. Wright), `valeo@pppl.gov` (E. Valeo), `ckphillips@pppl.gov` (C. Phillips) `bonoli@psfc.mit.edu` (P. Bonoli)

Abstract. Analysis of the propagation of waves in the lower hybrid range of frequencies in the past has been done using ray tracing and the WKB approximation. Advances in algorithms and the availability of massively parallel computer architectures has permitted the solving of the Maxwell-Vlasov system for wave propagation directly [Wright et al., Phys. Plasmas (2004), 11, 2473-2479]. These simulations have shown that the bridging of the spectral gap (the difference between the high injected phase velocities and the slower phase velocity at which damping on electrons occurs) can be explained by the diffraction effects captured in the full wave algorithm - an effect missing in WKB based approaches. However, these full wave calculations were done with a Maxwellian electron distribution and the presence of RF power induces quasilinear velocity space diffusion that causes distortions away from an Maxwellian. With sufficient power, a flattened region or plateau is formed between the point of most efficient damping on electrons at about 2-3 v_{the} and where collisional and quasilinear diffusion balance. To address this discrepancy and better model experiment, we have implemented [Valeo et al., "Full-wave Simulations of LH wave propagation in toroidal plasma with non-Maxwellian electron distributions", 18th Topical Conference on Radio Frequency Power in Plasmas, AIP Conference Proceedings (2007)] a non-Maxwellian dielectric in our full wave solver. We will show how these effects modify the electron absorption relative to what is found for a Maxwellian distribution.

---

1 Introduction

The wave equation finds much relevance in plasma physics. In this work we deal with externally driven radio frequency (RF) waves in the lower hybrid (LH) range of frequencies. This range is between the ion and electron cyclotron frequencies and is approximately given by $\omega_{lh} \approx \sqrt{\Omega_e \Omega_i}$ where $\Omega_{i,e} \equiv qB/m_{i,e}c$ are the electron and ion cyclotron gyration frequencies in a magnetic field of strength B. Because of the large mass ratio of protons to electrons, $Am_p/m_e \approx A1836$, this

results in a hybrid frequency that is much less than the electron cyclotron frequency and much greater than that of the ions', $\Omega_{ci} \ll \omega \ll \Omega_{ce}$. At these frequencies, the wavelengths are on the order of a few millimeters for parameters typical of fusion research devices, i.e. the magnetic field of the order of several Tesla and the electron density several times 10^{20} per m^3. The waves also have a high phase velocity on the order of 3-7 times the electron thermal velocity. This results in a high efficiency for driving toroidal current in the plasma [1, 2] which is needed for steady state stability of tokamak plasmas. For this reason, these waves have been proposed as a method of edge current profile control for the International Tokamak Experimental Reactor (ITER) [3]. LH experiments on Alcator C-Mod have achieved over 80% of the needed steady state current for the duration of the discharge, which represents several times that needed for current relaxation [4]. These experiments are at ITER relevant plasma parameters but the machine is about 10 times smaller than ITER making for more tractable sized simulations. Validation of our code on C-Mod LH experiments would support its use for predictive studies of LH on the ITER device now under construction.

The short wavelength relative to machine sizes of the order of a meter have encouraged the use of ray tracing as the primary method for calculating the power and current drive deposition in the plasma. The wavelengths are much shorter than the gradient scale length of the dielectric tensor, and so the Wentzel, Kramers and Brillouin (WKB) method would seem to be appropriate. While it can capture features such as broadening of the launched spectrum due to toroidicity [5] and the propagation path, it breaks down in cases where the rays undergo multiple reflections from cutoffs and caustics and form a stochastic field. Extended ray tracing techniques such as the Maslov method popular in seismology [6] and the wave-kinetic method [7], are valid at the caustic surfaces; but because the LH cutoffs in tokamak plasmas occur in the plasma edge where the gradients are very large, they violate the WKB approximation where the plasma is changing on the same scale as the wavelength [8].

A more serious challenge to traditional ray tracing is the importance of diffraction in LH wave

propagation [9, 10]. Although in LH experiments, frequencies are chosen to avoid the presence of any mode conversion, components of the wavenumber vector vanish at the caustics, and significant diffraction can occur there. There are other methods of dealing with high frequency waves that attempt to account for finite frequency effects such as diffraction [11] within the ray tracing picture. We have chosen to simulate the lower hybrid waves directly with the full wave code, `TORIC` [12], to account for these effects.

The outline of this paper is as follows. In Section 2 we describe the `TORIC` code and its discretization of the wave equation. In Section 3 the changes to the plasma model for the dielectric in the lower hybrid range of frequencies (LHRF) are given. We next discuss the inclusion of non-Maxwellian electrons in the plasma dielectric response in Section 4 - a critical requirement for waves with high phase velocities which cause large departures of the particle distribution from equilibrium. In Section 5 we discuss parallelization of the code. Section 6 concludes with a discussion of some possible applications and future improvements to the algorithm.

2   The wave equation and the `TORIC` code

The Maxwell-Boltzmann system in plasma physics reduces to a Helmholtz equation when modeling high frequency RF waves; essentially describing wave propagation in an anisotropic conducting media but with the non-local response of the plasma producing an integral form for the dielectric [13]. The wave amplitudes are taken to be small in the sense that three wave interactions play no role and we may linearize the Boltzmann equation. We assume that the equilibrium plasma quantitites are not changing on the time scale of wave propagation so the problem is represented in the frequency domain $E \sim \exp(i\omega t)$ and it is a partial differential equation in space only. This complex dielectric admits the existence of waves at widely disparate scales and different polarizations relative to the equilibrium magnetic field.

$$\nabla \times \nabla \times \mathbf{E} = \frac{\omega^2}{c^2} \left\{ \mathbf{E} + \frac{4\pi i}{\omega} \left(\mathbf{J}^{\mathrm{P}} + \mathbf{J}^{\mathrm{A}} \right) \right\} \tag{2.1a}$$

$$\mathbf{E}(\mathbf{x}) = \sum_m \mathbf{E}_m(r) \exp\left(im\theta + in\phi\right) \tag{2.1b}$$

$$k_\parallel = (m\mathbf{B} \cdot \nabla\theta + n_\phi \mathbf{B} \cdot \nabla\phi)/B \tag{2.1c}$$

$$\mathbf{J}_m^{\mathrm{P}}(r) = \sum_m \overset{\leftrightarrow}{\sigma}_c \left(k_\parallel^m, r \right) \cdot \mathbf{E}_m(r) \tag{2.1d}$$

The plasma wave equation that results [14] is given in Eq. (2.1a). The plasma response is embodied in the term $\mathbf{J}^P$ in Eq. (2.1d) and the type of wave generated is determined by the polarization of the electric field in the boundary condition set in the antenna current, $\mathbf{J}^A$ and the specified wave frequency, ω. In the case of a loop antenna, $\mathbf{J}^A$ determines a jump condition in the wave magnetic field (different from the plasma equilibrium magnetic field, $\mathbf{B}$) at the boundary that results in a Robin boundary condition due to the curvilinear toroidal coordinates (r, θ, ϕ). A wave guide source is represented by a Dirichlet boundary condition on $\mathbf{E}$ - the case we are concerned with in this paper. The plasma conductivity tensor is represented by $\overset{\leftrightarrow}{\sigma}_c$ and is simply related to the dielectric by $\overset{\leftrightarrow}{\varepsilon} = \overset{\leftrightarrow}{I} + \frac{4\pi i}{\omega} \overset{\leftrightarrow}{\sigma}_c$. It depends on the wavenumber, $k_\parallel$, from Eq. (2.1c) whose geometric dependence may be readily understood from its form in the limit of circular flux surfaces:

$$k_\parallel = \frac{m}{r} \frac{B_\theta}{B} + \frac{n_\phi}{R} \frac{B_\phi}{B}.$$

The currents represented by $\mathbf{J}^{\mathrm{P}}$ and $\mathbf{J}^{\mathrm{A}}$ are oscillating currents proportional to $\mathbf{E}$ and are distinct from the steady current induced in the electrons during current drive experiments that contributes to the confining magnetic field.

Equation (2.1b) shows how the problem is discretized by Fourier collocation in the periodic dimensions and cubic Hermite finite elements in the radial dimension. This representation also has the advantage of producing an algebraic representation of the parallel wavenumber [Eq. (2.1c)]

which is used in evaluating the conductivity in Eq. (2.1d). The resulting discrete system is solved by putting Eq. (2.1a) into Galerkin's weak variational form [12] which produces a dense block tridiagnonal system that is solved using the Thomas algorithm with the individual blocks being inverted with LU decomposition. In the ion cyclotron range of frequencies, the TORIC code is used routinely in a predictive mode and for analysis. It has been validated successfully on experiments on Alcator C-Mod [15, 16] has been compared against other codes [10, 17]. In the following sections we describe the extension of the plasma model for LHRF with non-Maxwellian electrons.

3   The plasma response model

In the lower hybrid range of frequencies, the ions are unmagnetized and effectively cold and the electrons are strongly magnetized $\left[(k_\perp \rho_e)^2 \ll 1\right]$. In Eq. (3.1) we consider the conductivity with thermal effects. The expressions for the plasma dielectric given in Eq. (3.3) and Eq. (3.1) are derived in references [12, 14] and correspond to the fourth and sixth order lower hybrid dispersion relations [18, 19] respectively when ∇ is replaced by the wavenumber, k.

$$\overset{\leftrightarrow}{\varepsilon} \cdot \mathbf{E} = S\mathbf{E}_\perp + iD(\mathbf{b} \times \mathbf{E}_\perp) + PE_\parallel \mathbf{b} + \nabla_\perp(\sigma\nabla_\perp \cdot \mathbf{E}) \tag{3.1}$$

$$S \approx 1 + \frac{\omega_{pe}^2}{\Omega_{ce}^2} - \frac{\omega_{pi}^2}{\omega^2} \tag{3.2}$$

$$D \approx -\frac{\omega_{pe}^2}{\omega^2}\frac{\omega}{\Omega_{ce}} + \frac{\omega_{pi}^2}{\omega^2}\frac{\Omega_{ci}}{\omega}$$

$$P = 1 - \frac{\omega_{pe}^2}{\omega^2} - \xi^2 Z'(\xi) \ \text{ where } \ \xi \equiv \omega/k_\parallel v_{the}$$

$$\sigma = \frac{3}{2}\frac{\omega_{pi}^2}{\omega^2}\frac{v_{thi}^2}{c^2}\left(1 + \frac{\omega^4}{\Omega_{ci}^2\Omega_{ce}^2}\frac{T_e}{4T_i}\right)$$

where S, D, and P, are the Stix cold plasma dielectric elements in the LHRF for the normal, co-

normal, and parallel directions [20], and $\omega_{\text{ps}}^2 \equiv 4\pi n_s q_s^2 / m_s$ is the plasma frequency for species s. The pressure driven term, σ, is the finite Larmor radius (FLR) correction to S and is responsible for the ion plasma LH branch. In regimes of experimental interest, σ is nearly vanishing and the ion plasma wave is strongly evanescent. In Eq. (3.1) and Eq. (3.3) below we have dropped the mode number suffixes but it should be understood that in general the coefficients $S, D, P,$ and σ are integral operators. The neglected FLR corrections to Eq. (3.3) support the mode converted ion plasma wave. Since this wave does not propagate for plasmas of experimental interest in which $\omega/\omega_{\text{LH}} > 2$ [19], we may neglect these corrections in the following analysis, and thus there are only two propagating modes, the fast electromagnetic LH branch that damps via electron Landau damping (ELD) and transit time magnetic pumping (TTMP) and the slow electrostatic LH branch that damps via ELD. Note, that although the FLR terms play no role, parallel thermal effects are kept through the plasma dispersion function in the ELD and TTMP damping in the plasma model.

Thus, we no longer need the ion finite thermal effects. After we drop the pressure driven term and therefore only solve for the fast and slow LH waves, the wave equation solved simplifies to

$$\nabla \times \nabla \times \mathbf{E} = S\,\mathbf{E}_\perp + \mathrm{i}D\left(\mathbf{b}\times\mathbf{E}_\perp\right) + P\,E_\parallel\mathbf{b}. \tag{3.3}$$

The neglected sixth order coefficient is proportional to $\beta\sqrt{\frac{m_e}{m_i}}$ in the LHRF and has no effect on the slow and fast branches. Here $\beta \equiv p/B^2$ is the ratio the plasma pressure and the magnetic field pressure. When the pressure driven term is set to zero, the equation for the radial component of the electric field is only related algebraically to the other two equations. This is a consequence of the nature of the Helmoltz operator, which does not have a radial derivative operating on E_r. It is necessary to remove E_r from the system of equations to avoid numerical pollution during the solution of the coupled finite element ordinary differential equations that result. This reduced system is much less stiff and results in a smaller matrix that is faster to solve by a factor of $(8/27)$ when using LU decomposition. The linear algebra for the reduction is done within the code. After

E_θ and E_ϕ are solved for, E_r is reconstructed.

4 Non-Maxwellian dielectric implementation

The dielectric response in the plasma is evaluated from velocity space integrals of a particle distribution function, $f_0(r, v_\perp, v_\parallel)$ [20]. In the specific case of a Maxwellian distribution this results in an infinite series of modified Bessel functions and Z-functions (also called the plasma dispersion function or Fried-Conte functions [21].) The presence of RF power causes velocity space diffusion that drives the distribution away from an Maxwellian. With sufficient power, a region of reduced slope or plateau is formed by this RF quasilinear diffusion between the point of most efficient damping on electrons at about $v_\parallel \approx 2 - 3v_{\text{the}}$ and where collisional and quasilinear diffusion balance [22, 23]. When we neglect finite Larmor radius effects in the LHRF, the Bessel functions are reduced to a single coefficient, but we are still left with evaluating the generalized plasma dispersion function. For the purposes of this paper, we will use the evaluation of the $\varepsilon_{\parallel,\parallel}$ component of the dielectric, where $\parallel$ denotes the direction parallel to the equilibrium magnetic field. The derivation presented below closely follows that of Valeo [24].

$$\varepsilon_{\parallel,\parallel} = 1 + \frac{2\omega_p^2}{k_\parallel w_\perp^2} \left[B(\xi) + \int d\mathbf{v} \frac{v_\parallel}{\omega} f_0(\mathbf{v}) \right] \tag{4.1}$$

$$B(\xi) \equiv 2\pi \int_{-\infty}^{\infty} dv_\parallel \frac{v_\parallel}{\omega - k_\parallel v_\parallel} \int_0^{\infty} dv_\perp v_\perp H(v_\parallel, v_\perp) \tag{4.2}$$

In Eq. (4.1), $w_\perp$ is the perpendicular variance of the distribution; for a Maxwellian distribution $w_\perp = v_{\text{the}}$. The first term in brackets poses the most difficulty in evaluation because it has a pole as shown in Eq. (4.2). $H(v_\parallel, v_\perp)$ is non-singular and closely related to f_0 and is given in Equation 10.50 of Stix [20]. What is important to note is that the perpendicular velocity space integrals produce smoothly varying functions of $v_\parallel$ whose product with the singular function $w(v_\parallel) = (\omega -$

$k_\parallel v_\parallel)^{-1}$ must then be integrated in $v_\parallel$. If f_0 is Maxwellian, then these parallel velocity space integrals can be represented in terms of the plasma dispersion function $Z(\omega/k_\parallel v_{\text{the}})$. Our goal is to evaluate Eq. (4.2) efficiently for arbitrary f_0.

In the integral over $v_\perp$ in Eq. (4.2) the factor $w(v_\parallel)$ is a singular weight function and the remaining part of the integrand, which we represent by $C(v_\parallel) = v_\parallel \int_0^\infty dv_\perp v_\perp H(v_\parallel, v_\perp)$, is smooth. Therefore, $B(\xi)$ will be smooth and we are justified in tabulating it on a uniform mesh, $\xi = x_j$, where x_j is a velocity mesh coordinate normalized to v_{the}. We evaluate $C_j = C(v_\parallel/v_{\text{the}} = x_j)$ on the same mesh with a simple linear tent function in Eq. (4.3) for interpolation. The weight function is also made discrete with $w_j = w(v_\parallel/v_{\text{the}} = x_j)$.

$$T_j = \begin{cases} 1 - \frac{|x-x_j|}{\Delta} & \text{if } |x - x_j| \leq \Delta \\ 0 & \text{otherwise} \end{cases} \tag{4.3}$$

$$K_j = \int_{-1}^1 dv \frac{1-|v|}{v+j} = \begin{cases} \ln\left(\frac{j+1}{j-1}\right) - j \ln\left(\frac{j^2}{j^2-1}\right) & |j| > 1, \\ \pm \ln 4 & j = \pm 1, \\ i\pi & j = 0. \end{cases} \tag{4.4}$$

The evaluation of $B(\xi)$ in Eq. (4.2) now can be reduced to a known integral of interpolating tent function T_i and the discrete singular weight function, w_j. This known integral is the kernel function, K_j in Eq. (4.4). The evaluation of B in Eq. (4.2) now results in a convolution between C_i and K_j.

$$B(\xi/v_{\text{the}} = x_k) = B_k = \sum_i C_i K_{i-k} \tag{4.5}$$

This technique has been verified by comparing results for a Maxwellian velocity distribution for which $B(\xi)$ should be Z functions. The computational cost of the general technique is quite modest. For example, a mesh of 200 points for the parallel velocity grid takes about four times as long as for the analytic evaluation employing the Z function. As this is only a portion of the
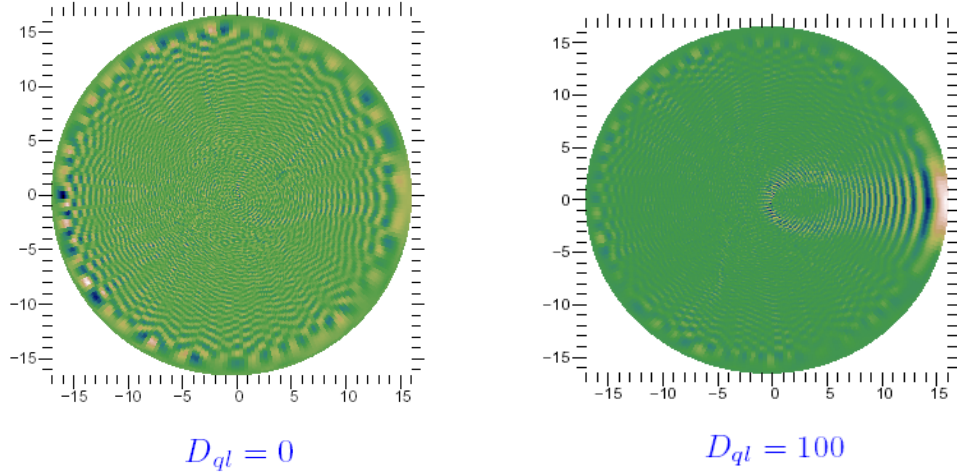
$D_{ql} = 0$ $D_{ql} = 100$

Figure 1: Left figure: $E_\parallel$ for a Maxwellian distribution. Right figure, $E_\parallel$ with a quasilinear plateau. The enhancement of absorption is clearly evident. The parameters used are characteristic of Alcator C with central magnetic field of $10T$, central density of $5 \times 10^{19} m^{-3}$, central temperature of 1.8 keV. With a parallel index of 1.87 at the waveguide mouth. Major/minor radii of R/a = 66cm/16.5cm Profiles are simple double parabolic: $f(r/a \equiv x) = (1 - x^2)^2$.

overall calculation and its cost is fixed as the spatial resolution increases, it's impact on run time is vanishing for large problems. Applied to a test non-Maxwellian distribution, we can see the importance of including the generalized dielectric. In the plots of $Re(E_\parallel)$ in Fig.(1), with non-zero quasilinear diffusion (D_{QL}), a plateau tail is formed for values of $v_\parallel / v_{the}$ between 2.2 and 8. The magnitude of D_{QL} determines how flat the plateau is and there is no appreciable change in the results for larger values. We can see that for a Maxwellian, the absorption is fairly weak and almost a standing wave pattern is set up, while in the presence of the wave induced velocity space diffusion, strong absorption in front of the waveguide (midplane on the right side of the contour plots) is seen. The plasma parameters were chosen to accentuate this effect having low damping due to the relatively low temperature and density.
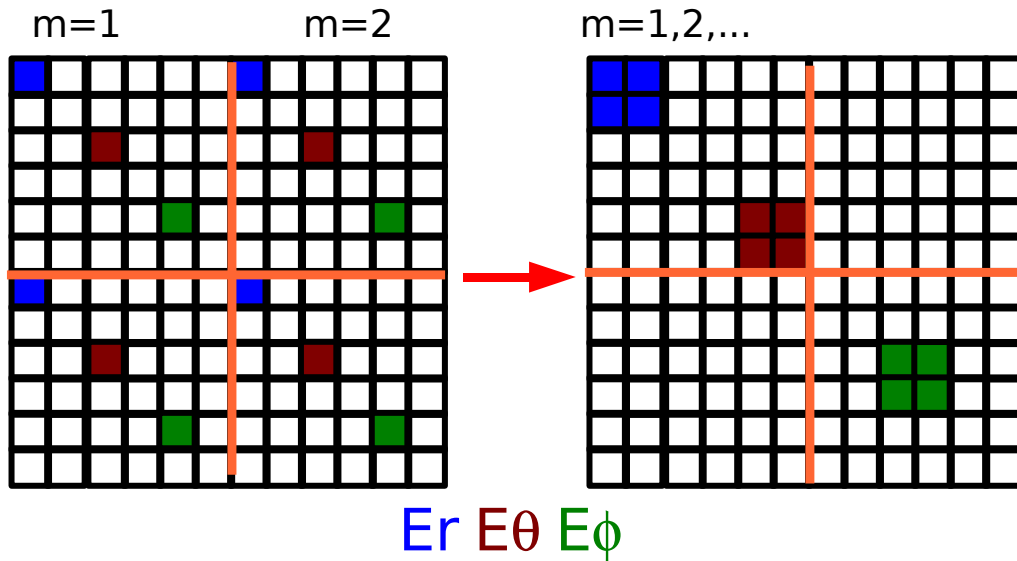
Figure 2: Diagram of the reordering of matrix elements needed for elimination of E_r in the lower hybrid algorithm. The red solid lines separate the stiffness matrix into four cpu regions. For construction and solution each cpu has all field components at a mesh point or points for most efficient communication as in the left example. On the right, the matrix has been reordered so that each field components representation is logically continuous in the distributed matrix.

5   Parallelization and convergence

When we examine the required resolution for LH simulations even for smaller research tokamaks, we quickly conclude that a parallel version is needed both for memory requirements and reasonable executions times. The worst case for poloidal resolution is at the caustics where k_r vanishes and $k_\perp \approx m/r$. The number of modes needed depends on radius with the most restrictive condition at the plasma edge. Taking $k_\perp = 2\pi/1$mm and $r = a = 20$ cm we estimate $N_m \approx 1200$. If we take $\lambda_r \approx 1$ mm as a typical radial wavelength and require 2 cubic elements per wavelength, the requirement is for 400 radial elements for the same minor radius. The scalar version of the TORIC code accepts any problem dimension but is limited to memory requirements of array storage. Using out-of-core techniques can extend the resolution about another factor of two in each dimension, but then the processing time becomes burdensome (due to problem size, not the out-of-core disk access). The practical effect is that given 2GB of RAM memory, the problem size is restricted

to approximately 400 radial elements with 255 poloidal modes, or half that in both dimensions if the out-of-core technique is not used. Parallelization is clearly required to achieve the necessary resolutions for lower hybrid simulations.

The previous ion cyclotron version of `TORIC` has already been parallelized [17, 25]. Parallelization is done in the poloidal dimension for matrix inversion of the resulting block tri-diagonal system with `ScaLAPACK` [26] and along the radial dimension during processing of the solution for power and current drive deposition. The added complication introduced by the LH version is associated with the elimination of E_r - the diagram in Fig. 2 illustrates the issue. For the purposes of the construction of the stiffness equation it is most efficient to have each electric field component and it's derivative on the same cpu. During the elimination and post calculation of E_r we need to invert the sub-matrix representing the coefficients of E_r in the stiffness matrix. Since `ScaLAPACK` only can do this for stride one distributed matrices, the matrix must be reordered so that the needed coefficients are logically contiguous. The parallel version has been verified for small problems against the serial version of the code. Cross verification against ray tracing has shown diffraction to have significant effects on drive heating and current profiles [10].

Lower hybrid simulations require high resolution, particularly in the direction parallel to the equilibrium magnetic field to resolve all the important scales. Such large simulations are only possible on large parallel systems. As Fig. 3 demonstrates, two thousand poloidal modes can easily be required to resolve lower hybrid waves in a high field tokamak. At the antenna, the spectrum is narrow and peaked about $m = 0$, i.e. the launched $n_\parallel$ determined by the toroidal mode number. By $r/a \sim 0.8$ diffraction has broadened the spectrum to $m \sim 800$ and most of the wave energy has been absorbed. The two primary reasons for the large amount of resolution needed are that the wave scale itself is small and the parallel phase velocity at which damping occurs has to be resolved. For the Alcator C-Mod tokamak used in this simulation, the wavelength is on the order of a millimeter the minor radius of 22 cm. With two cubic elements per wavelength, we require a minimum of 600 radial elements. In addition, waves will diffract while propagating

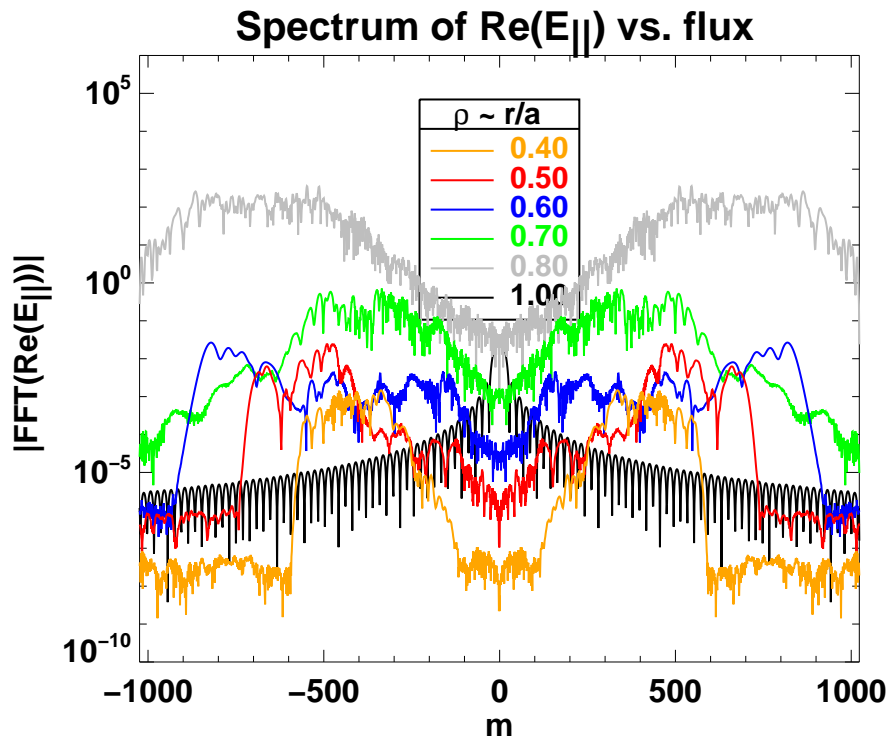## Spectrum of Re(E$_{||}$) vs. flux

Figure 3: A measure of spectral convergence in poloidal dimension. The case presented is an experimentally relevant scenario on the Alcator C-Mod tokamak. The plasma parameters used are a magnetic field of 5.5 Tesla, electron density of $7 \times 10^{19} \mathrm{m}^{-3}$, and electron temperature of 5 keV and a deuterium plasma. Values given are the at the center of the device. Wave frequency is 4.6 GHz and parallel index is 2.55. The resolution used is 980 radial elements and 4096 poloidal grid cells which permits 2047 poloidal Fourier modes.

until their parallel phase velocity is on the order of a few times the thermal electron velocity, $\omega/k_\parallel \sim 3v_{\mathrm{the}}$, at which point they will damp. Since $v_{\mathrm{the}} \equiv \sqrt{k_B T_e/m_e} \approx 42\sqrt{T_e}[\mathrm{keV}]$ where k_B is the Boltzmann constant, we can write this as a condition on the parallel index of refraction, $n_\parallel \equiv k_\parallel \omega/c$: $n_\parallel \approx 5.4/\sqrt{T_e[\mathrm{keV}]}$. So for absorption in the outer parts of the plasma where the temperature may be of the order of 1 keV or less, the parallel index must shift to values greater than 5. Consulting Eq. (2.1c) we see this translates directly to increased poloidal resolution.

6   Discussion

The parallel algorithm is capable of the required resolutions for Alcator C-Mod which has similar LH wave dispersion as in ITER. Recent hard X-ray (HXR) measurements on C-Mod show consistent differences from synthetic diagnostics using ray tracing [4]. In brief, the measurements are broader with a larger integrated signal than the simulations, indicating that deposition layer is further out in minor radius with a more intense field. This is consistent with observed differences between full wave and ray tracing calculations - in full wave simulations diffraction causes a large upshift in the parallel wavenumber shifting the resonant phase velocity downwards, and so the waves damp on cooler electrons that are at larger minor radii. We plan next to investigate this case in detail with the parallel solver. This work will also require coupling the non-Maxwellian dielectric to a Fokker- Planck solver via a quasilinear diffusion operator. For this step we would leverage previous work coupling the `AORSA` full wave code and the `CQL3D` Fokker-Plank code [27] under the US RF- SciDAC project.

We have described a new tool for understanding lower hybrid physics in tokamaks. A full wave code `TORIC` with non-Maxwellian electrons will be able to investigate heating and current drive scenarios in tokamaks without using the WKB approximation. Coupling to a Fokker-Planck code will permit self-consistency between the fields and the distortion of the distribution. Discrepancies in recent Alcator C-Mod experiments with simulation motivate applying this tool to better understand the HXR measurements. Accurate understanding of the role of diffraction in determining the location of current drive could have important impacts on the implementation of lower hybrid in ITER.

Acknowledgments

References

[1] Karney, C. F. F. and Fisch, N. J., Phys. Fluids **29** (1986) 180.

[2] Fisch, N. J., Rev. Mod. Phys. **59** (1987) 175.

[3] ITER Physics Expert Group on Energetic Particles, Heating and Current Drive and ITER Physics Basis Editors, Nucl. Fusion **39** (1999) 2495.

[4] Bonoli, P. T. et al., Phys. Plasmas **15** (2008) 056117.

[5] Bonoli, P. T. and Ott, E., Phys. Fluids **25** (1982) 359.

[6] Chapman, C. H. and Keer, H., Stud. Geophys. Geo. **46** (2004) 615.

[7] Kupfer, K., Moreau, D., and Litaudon, X., Phys. Fluids B **5** (1993) 4391:4407.

[8] Brambilla, M. and Cardinali, A., Plasma Phys. **24** (1982) 1187.

[9] Pereverzev, G. V., Nucl. Fusion **32** (1992) 1091.

[10] Wright, J. C. et al., Full-wave electromagnetic field simulations of lower hybrid waves in tokamaks, in *16th Topical Conference on Radio Frequency Power in Plasmas*, edited by Bonoli, P. and Wukitch, S., number 787, page 287, New York, 2005, American Institute of Physics.

[11] Runborg, O., Commun. Comput. Phys. **2** (2007) 827.

[12] Brambilla, M., Plasma Phys. Controlled Fusion **41** (1999) 1.

[13] Stix, T. H., *Waves in Plasmas*, chapter 10, page 250, In stixwaves [20], 1992.

[14] Brambilla, M., Plasma Phys. Controlled Fusion **31** (1989) 723.

[15] Lin, Y. et al., Plasma Phys. Controlled Fusion **47** (2005) 1207.

[16] Lin, Y. et al., Plasma Phys. Controlled Fusion **45** (2003) 1013.

[17] Wright, J. C. et al., Phys. Plasmas **11** (2004) 2473.

[18] Stix, T. H., Phys. Rev. Lett. **15** (1965) 878.

[19] Bonoli, P., IEEE Trans. Plasma Sci. **PS-12** (1984) 95.

[20] Stix, T. H., *Waves in Plasmas*, American Institute of Physics, New York, 1992.

[21] Fried, B. and Conte, S., *The Plasma Dispersion Function*, Academic Press, New York, New York, 1961.

[22] Kennel, C. F. and Engelmann, F., Phys. Fluids **9** (1966) 2377.

[23] Fisch, N. J., Phys. Rev. Lett. **41** (1978) 873.

[24] Valeo, E. J. et al., Full-wave simulations of icrf heating in toroidal plasma with non-maxwellian dis-

tribution functions, in *Program of the 48th annual meeting of the Div. of Plasma Physics*, volume 51, pages VP1–47, Philadelphia, PA, 2007, Bull. American Phys. Soc.

[25] Wright, J. C., Bonoli, P. T., Azevedo, E. D., and Brambilla, M., Ultrahigh resolution simulations of mode converted icrf and lh waves with a spectral full wave code, in *Proceedings of the 15th Conference on Radio Frequency Power in Plasmas*, edited by Forest, C. B., number 694, pages 511–514, New York, 2003, American Institute of Physics.

[26] Choi, J. et al., Scientific Programming **5** (1996) 173.

[27] Jaeger, E. F. et al., Nucl. Fusion **46** (2006) S397.